

We are IntechOpen, the world's leading publisher of Open Access books Built by scientists, for scientists

6,900

Open access books available

186,000

International authors and editors

200M

Downloads

Our authors are among the

154

Countries delivered to

TOP 1%

most cited scientists

12.2%

Contributors from top 500 universities



WEB OF SCIENCE™

Selection of our books indexed in the Book Citation Index
in Web of Science™ Core Collection (BKCI)

Interested in publishing with us?
Contact book.department@intechopen.com

Numbers displayed above are based on latest data collected.
For more information visit www.intechopen.com



AFM Imaging of Biological Supramolecules by a Molecular Imprinting-Based Immobilization Process on a Photopolymer

Taiji Ikawa

*Toyota Central Research and Development Laboratories, Inc.
Japan*

1. Introduction

Biologically derived molecules (biomolecules) are extremely diverse in their physical sizes, chemical and structural properties. They form supramolecular assemblies *in vivo/vitro* through noncovalent interactions (e.g., hydrogen bonding, hydrophobic interactions, π - π interactions, and/or electrostatic). The structures of the supramolecular assemblies change with the concentrations of salts and the biomolecules itself. Efficient immobilization of various biomolecules and their assemblies is a key aspect of many applications including microarray technologies, (Kambhampati (Ed.), 2003; Schena (Ed.), 2004) biotechnology in general (Mayers, 2002; Whitesides, 2001) and structural analysis based on AFM.

Structures and functions of the biomolecules and their assemblies are susceptible to physical and chemical surface properties and nanotopography of the substrate, and such interfacial forces effect a nanoscale change in molecular shape and structure. (Ostuni, et al., 2001; Ramsden, 1993; Wahlgren & Arnebrant, 1993) The first problem to be overcome is the tendency for biomolecules to denature on contact with the substrate surfaces. Extensive approaches have been developed, using either covalent attachment or noncovalent affinity binding (Mayers, 2002). The covalent coupling process can achieve stable coupling, but it needs complexity and cost of derivation steps, and limited sites for attachment leads to shorter lifetime. The process has a possibility of denaturation by the chemical treatment. On the other hand, the noncovalent affinity binding process is the simplest approach to the immobilization but it tends not to be stable, and activity of biomolecule is often lost in time-dependent structural changes (Ramsden, 1993). For example, mica surface provides an atomically flat surface, but the surface repels most of the biomolecules due to its negative charge. Multivalent cation or chemical modification process are used to avoid repulsion (Bezanilla et al., 1995; Hansma, 2001; Lamture et al., 1994), however, the structures of the supramolecular assemblies changed with the concentrations of salts (Wong et al., 2003).

A recent study for the noncovalent affinity binding process has been directed toward the selective adsorption of biomolecules using nanopatterned surfaces (Cunin et al., 2001; Curtis & Eilkinson, 2001; Shi et al., 1999) and/or molecularly imprinted polymers (Alexander et al., 2003; Haupt, 2003) so as to hold the 3-dimensional structure of the biomolecules. However, these approaches have met with limited success due to their complicated chemical processes and the often expensive facilities required for nanofabrication.

In this chapter, a new technique for the noncovalent immobilization of the biomolecules using a polymer containing azobenzene moiety (azopolymer) is presented (Ikawa et al. 2006, 2007, 2010). The principle of the technique is simple; the azopolymer surface deforms along contours of nano-scale macromolecules during photoirradiation, effectively immobilizing the macromolecules without chemical modification (Fig. 1). That means the molecular shape is imprinted on the azopolymer surface by the photo-irradiation.

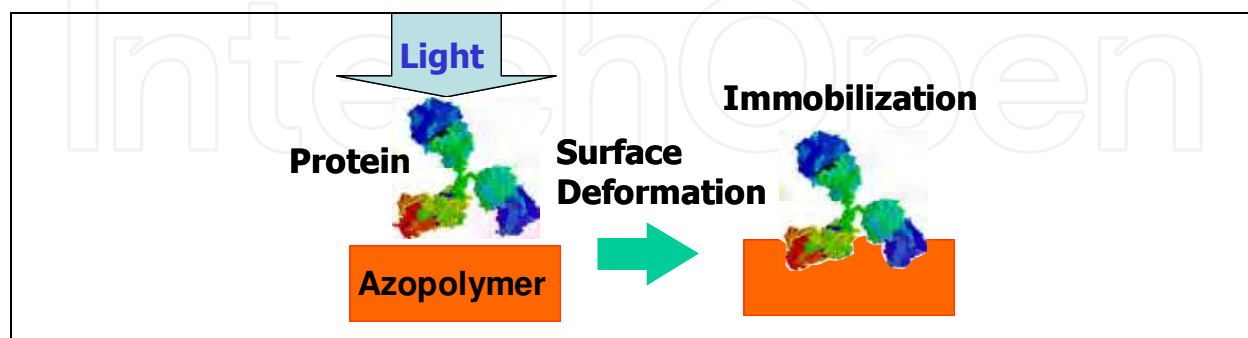


Fig. 1. Principle of the immobilization of protein.

The technique is well suited for imaging biomolecules, especially for AFM, providing a non-reactive, non-ionic, and flat surface (the surface roughness can be < 0.3 nm) on which the complex supramolecular assemblies can be immobilized with little conformational change in the native aqueous environment. The immobilization process dramatically reduces the thermal motion of biomolecules, leading to higher imaging resolution allowing individual biomolecules to be resolved.

The nano-scale biomolecules such as deoxyribonucleic acid (DNA), immunoglobulin G (IgG), and tobacco mosaic viruses (TMV) are demonstrated to be immobilized on such an azopolymer surface by photoirradiation because of a topographic change in the azopolymer surface with the biomolecules after photoirradiation. The imaging technique is also shown to investigate the phase behaviour of cytoskeletal muscle protein aggregates as a function of concentration of the multivalent cation. The data provided direct experimental evidence of a coil-on-coil (braided) structure and the two dimensional nematic rafts discovered by recent x-ray studies (Wong, 2003) and theoretical treatments (Borukhov,1997).

2. Principle of the immobilization of biomolecules on the azopolymer

2.1 Photoinduced motions in azopolymer

2.1.1 Photoisomerization of azobenzenes

Azobenzene and its derivatives can exist in two forms that differ in the isomerization state of the azo group ($-N=N-$) (Fig. 2) (Rau, 1990). One is the trans-form, which has the stable rod-like form in shape. The other is the cis-form, which has the relatively unstable bent form. The stable trans-form isomerizes into the unstable cis-form when the azobenzenes absorb light. Cis to trans back isomerization can take place thermally and/or photochemically.

Azobenzenes have been classified into three groups by spectroscopic analysis: azobenzene-type molecules, aminoazobenzene-type molecules and pseudo-stilbene-type molecules (Fig. 2)

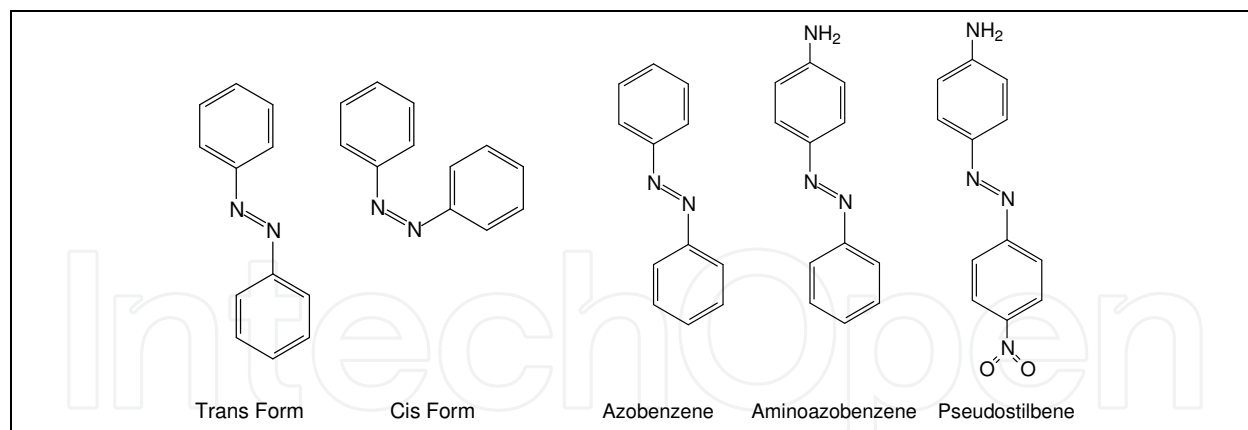


Fig. 2. Isomers of azobenzene and three groups of azobenzene derivatives.

(Natansohn & Rochon, 2002; Rau, 1990). Azobenzene-type molecules have two absorption bands due to $\pi\text{-}\pi^*$ and $n\text{-}\pi^*$ transition with relatively poor overlap between the two bands. The lifetime of the cis isomer is relatively long up to hours and more. Aminoazobenzene-type molecules show significant overlap of the two absorption bands and the lifetime of the cis isomer is shorter. Pseudo-stilbene-type molecules, where 4- and 4'-positions of the two azobenzene rings are substituted with electron-donating and electron-withdrawing groups, has the two bands overlapped on around the same energy level and the lifetime of the cis isomer is shortest up to second range. Since the $\pi\text{-}\pi^*$ and $n\text{-}\pi^*$ bands are practically superimposed, light for photoactivation of the trans-cis isomerization will also photoactivate the cis-trans isomerization, which will significantly speed up the whole process. The process can be repeated under illumination, and thus, pseudo-stilbene-type molecules are the best molecules for inducing drastic changes to their surrounding matrix.

2.1.2 Photoisomerization-induced motions in azopolymer

Azobenzenes undergo repeated photoisomerization during photoirradiation even in a glassy-state polymer. Nonbound azobenzenes can affect their environment if they are dissolved in a polymer matrix. The molecular motions of azobenzenes induce the multi level motions in the polymer. The motions can be roughly classified into the following three types (Natansohn & Rochon, 2002).

The first type of motion is the photo-induced orientation of chromophores in a polymer matrix. With linearly polarized light, the photoisomerization is only activated when the chromophore's transition dipole moment axis has a component parallel to the light polarization. The direction perpendicular to the light polarization is excluded from optical activation and become enriched in chromophores. The concentration of the chromophores aligned perpendicular to the light polarization steadily increases under illumination with polarized light, until a saturation level is attained. This motion produces dichroism and birefringence in polymers (Todorov et al., 1984). Pseudo-stilbene-type azobenzenes is the best molecule for inducing photo-induced orientation because of their fast isomerization process. Aminoazobenzenes are good candidates for the motion, but azobenzenes shows little photoinduced orientation due to their slow back isomerization process.

The second type is domain level motions in conjunction with chromophore motions. To induce this type of motion, the azobenzenes should be part of ordered and/or constrained

matrix, for example, liquid crystalline, semi crystalline, Langmuir-Brodgett or monolayer films. Any type of azobenzenes are useful for inducing this kind of motion. In case the azobenzenes undergo photo-isomerization and alignment in the constrained matrix, liquid crystals domains reorient to a direction perpendicular to the light polarization (Ichimura, 2000). Also, the photoisomerization can act as a trigger to disrupt an ordered phase of liquid crystals, which is the most common case found in the literature. The difference in shape between the E (trans) azobenzene isomer and the Z (cis) provides a powerful mesogen (E) and an effective liquid crystalline phase disruptor (Z, with some exceptions).

The third type is massive macroscopic motion at an even larger scale. The photo-illumination with interference pattern of the laser beams produces relief patterns on the polymer surface (Fig. 3) (Kim et al., 1995; Rochon et al., 1995). Direct exposure to the laser beam also forms a dent structure on the polymer surface. To induce this kind of motion, pseudo-stilbene-type azobenzenes is the best molecule and it requires that the azobenzenes should be connected to polymers. This motion has been considered to be a photo-driven mass transport effect because total volume of the polymer is almost the same after photo-illumination, which is quite different from other conventional microscopic surface processing. Various driving forces behind it have been proposed such as internal pressure (Rochon et al., 1995), light intensity gradient (Kim et al., 1995), and intermolecular interaction (Pedersen et al., 1997). However, neither the mass transport effect itself nor the nature of the driving force has been directly confirmed. Recently, Karageorgiev et al. reported the observation of light-induced isothermal transition of the polymer film from a solid phase to a fluid phase by atomic force microscopy (Karageorgiev et al., 2005). In their report, the polymer behaves like a viscoelastic fluid during photo-illumination, whereas the fluidity is affected by the light field vector. The result suggests that the photoisomerization motion of the azobenzene plasticizes the polymer matrix during photo-illumination, which is considered to be the first step of the massive macroscopic motion of the polymer.

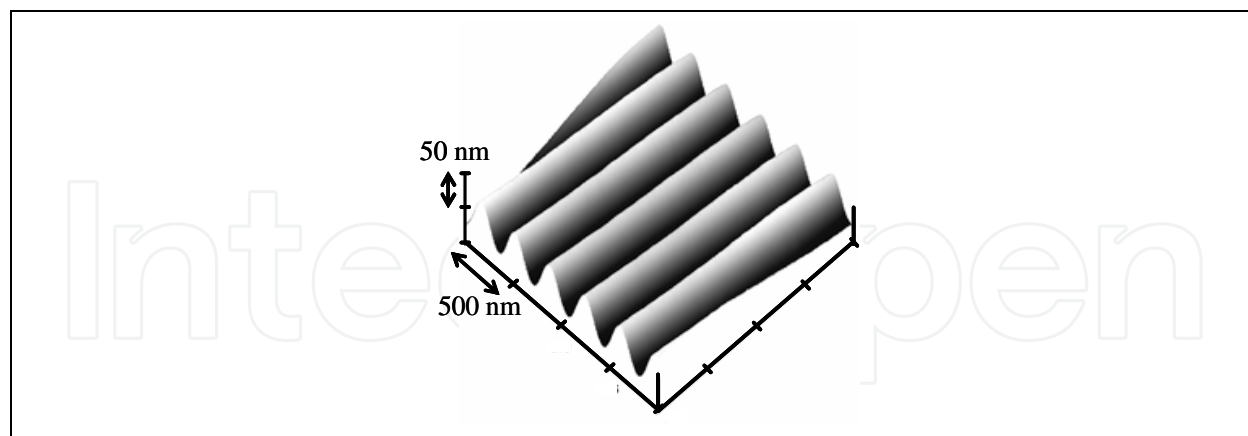


Fig. 3. A relief pattern formed on an azopolymer surface by exposure to an interference pattern of light, imaged by atomic force microscopy.

2.1.3 Surface deformation of azopolymers by sub-micron sized dielectric particle

The author's research group found that a topographical change could be induced on the surface of azobenzene-containing polymers by means of photo-illumination with a monolayer of polystyrene (PS) particles of submicron diameter (Hasegawa, 2001; Ikawa et

al. 2000; Kawata et al., 1999). The experimental technique to display this phenomenon is very simple: (1) a monolayer of PS particles was formed on the surface of the azopolymer film; (2) the polymer film was exposed to a laser beam; (3) after removing the particles, hexagonally arrayed dents, of which diameter were nearly the same as the PS particles, were formed on the surface (Fig. 4). The dents structure with a diameter from 1000 nm to 20 nm could be achieved. The author explored the mechanism of the nanoscale deformation of the azopolymer based on (1) size effects of the small particles on the nanostructure formation, (2) the electric field calculated by Mie scattering theory, and (3) the visco-elasticity analyzed by scanning probe microscopy (Ikawa, 2001). The result implies that "the optical near field" of the PS particles that are smaller than the wavelength of the incident light can cause the nano-scale surface deformation of the azopolymer. This technique itself was considered to be an entirely new nano-structure fabrication technique, and showed the potential of the azopolymer for the application to near-field imaging (Kawata, 1999) and optical data storage (Hasegawa, 2001).

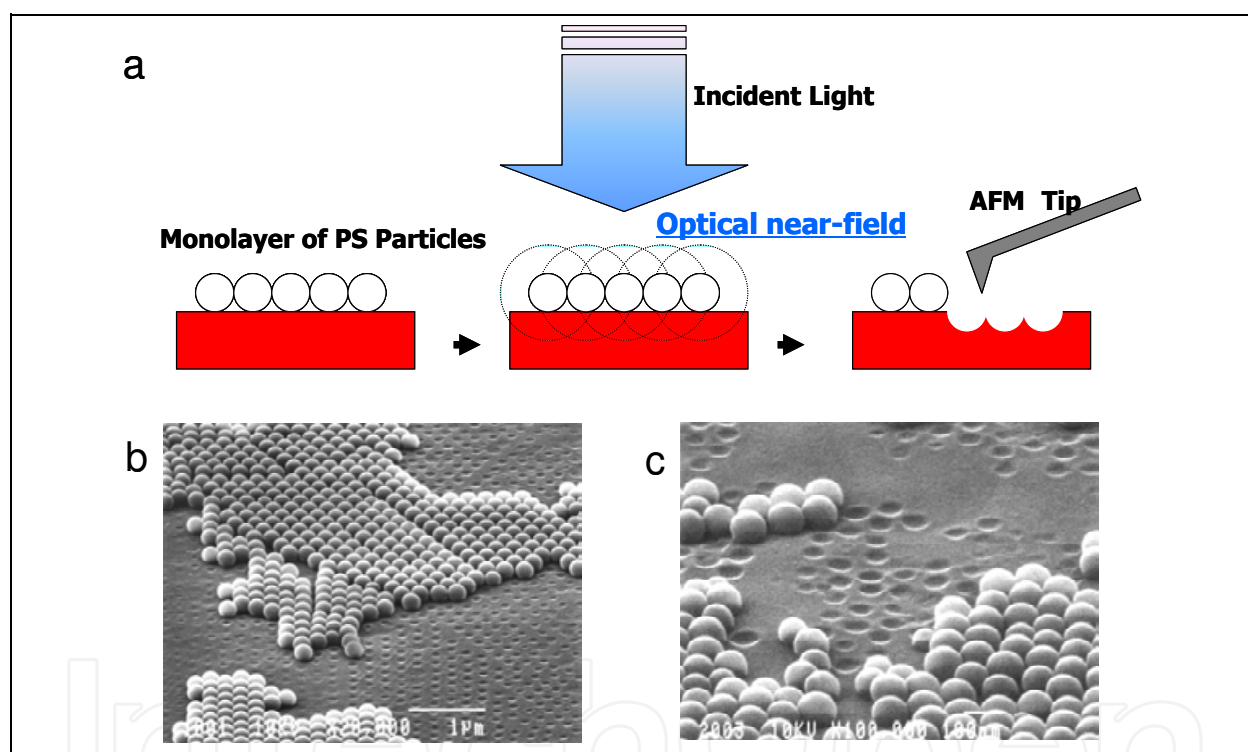


Fig. 4. (a) Schematic representation of the nanostructure patterning by spherical particles. (b) and (c) SEM images of the azopolymer surfaces treated by (b) the particles of 241 nm in diameter and (c) the particles of 98 nm in diameter. The particles were partially removed from the surface by sonication.

2.2 Immobilization of small particles on the azopolymer surface and AFM imaging

In the course of these studies, the author found that the small particles on the azopolymer can be immobilized by photo-illumination (Ikawa, 2006). As shown in Fig. 4, the deformed surface is considered to effectively sustain the particles. Of particular interest is that not only PS particles but biomolecules including globular proteins, filamentous proteins and deoxyribonucleic acids (DNA) can be immobilized on the azopolymer.

The author confirmed that the azopolymer surface deforms along the shapes of the small particles, suggesting that the small particles are physically immobilized on the surface because of the increase in the contact area between the small particles and the polymer. The immunological and enzymatic studies showed that the immobilized proteins keep their vital activities (Ikawa, 2006). This new concept for the immobilization of the biological macromolecules has the distinct potential for biological applications including protein chip application (Mouri, 2010) and biological imaging (Ikawa, 2007). Moreover, it provides a new concept of the fabrication of two-dimensional array of spherical particles (Watanabe, 2010).

Following section, nano-scale particles including both deoxyribonucleic acid (DNA) and proteins are shown to be immobilized on the surface of the azopolymer only by photoirradiation. Atomic force microscopy (AFM) reveals that the polymer surface deforms along the contour of the nano-scale particles and physically holds them upon photoirradiation. Immunological and enzymatic studies present that proteins immobilized on the polymer surface retained their original functionality.

2.2.1 Experimental technique: Preparation of azopolymer films and photoimmobilization of biomolecules on the films

Two kinds of azopolymers were used in the experiment. **Polymer 1:** A urethane-urea copolymer containing disperse red 19 was synthesized (Ikawa et al., 2001; Kawata et al., 1999). The polymer had a molecular weight of 170,000 (relative to polystyrene), a glass transition temperature (T_g) of 145°C and an absorption maximum of 475 nm. Contact angles of water and ethylene glycol to the polymer were 83° and 58°, respectively. Changes in the absorption spectrum and the contact angles cannot be detected before and after 1-hour photoirradiation with 25 mW/cm² of light from a 5x10 arrays of blue light emitting diodes (LEDs, Toyoda Gosei). The absorbance at a wavelength of 470 nm for the film was 5% lower than the absorbance at the wavelength of 475 nm (λ_{max}). UV-vis absorption spectra of the film before and after photoirradiation were obtained by a Shimadzu UV-2000 spectrophotometer. **Polymer 2:** Poly{4'-[[[2-(methacryloyloxy) ethyl]ethyl] amino]-4-cyanoazobenzene-co-methyl methacrylate} (15 mol% azobenzene moiety) was obtained by free-radical polymerization (Ikawa, 2006 and 2010). The polymer had a molecular weight of 25,000, a T_g of 102°C and an absorption maximum of 447 nm. Contact angle of water and ethylene glycol to the polymer were 75° and 53°, respectively. Changes in the absorption spectrum and the contact angles cannot be detected before and after 1-hour photoirradiation with 25 mW/cm² of light from LEDs. The absorbance at a wavelength of 470 nm for the film was 10% lower than the absorbance at the wavelength of 450 nm (λ_{max}). The 50 nm-thick azopolymer films were prepared on amino-conjugated glass slides by spin coating from a pyridine solution. Mean roughnesses (R_a) of the bare azopolymers surfaces were around 0.6 nm, being about the same before and after photoirradiation without those biomolecules.

Changes in the azopolymer surface topography with λ -DNA, Immunoglobulin G (IgG), and Tobacco mosaic virus (TMV) before and after photoirradiation were probed by atomic force microscopy (AFM). **λ -DNA:** An aqueous solution of 1 mg/mL λ -DNA was spin-coated onto the azopolymer (polymer 1) surface and then the surface was irradiated with laser light of 488 nm in wavelength and 10 mW/cm² in optical power densities for 10 min. The surface was observed by contact-mode AFM (Digital Instruments Nanoscope E) and a silicon nitride cantilever (the typical tip radius of curvature is 15 nm, Nanoworld). **IgG:** 1 μ L of a

phosphate buffered saline solution (PBS) containing fluorophore (Cy5)-linked IgG (Funakoshi) was spotted on the azopolymer (polymer 2) surface. After evaporating the solution, the surface was irradiated with light from the 5x10 arrays of blue LEDs for 30 min; optical power density at the polymer surface was measured by an Ophir optical power meter and was around 25 mW/cm². Then, the surface was washed for 30 min with PBS containing 0.01 wt% Tween20 as a nonionic surfactant. The amount of the immobilized IgG was confirmed by the fluorescence intensity of the spot. The fluorescence intensity increased linearly with the concentration of IgG in the spotting solution and saturated around 2 µg/mL. Under this condition, the area density of IgG on the spot was about 2.5 ng/mm², corresponding to the amount calculated for a close-packed monolayer of IgG. For the AFM experiments, the spotting solution containing 0.5 µg/mL IgG was selected, so as to avoid the formation of the multilayer. The surface image was obtained by tapping-mode AFM (Digital Instruments, Dimension 3100) and a sharp silicon cantilever (the tip radius of curvature is under 5 nm, Nanoworld). The azobenzene-containing polymer surface was then washed with PBS containing 2 wt% of sodium dodecyl sulfate (SDS) to remove IgG. After confirming that the fluorescence from the spot had disappeared, a further AFM image was obtained. **TMV:** TMV was purchased from BIOREBA AG. Purification of TMV was performed by a Beckman XL-90 ultracentrifuge system. Stock solution of TMV was desalted and diluted by buffer exchange using Milipore Micocon YM-10 filter units. The final concentration of the TMV solution was 5.5 µg/mL of TMV and 10 µM of PBS. 2 µL of working solution was spotted on the azopolymer film, and then the solution was dried naturally. The film was then irradiated with light at a wavelength of 470 nm from an array of blue LEDs (25 mW/cm²). The film surface was observed by a contact-mode AFM (Nanoscope E, Digital Instruments) with a silicon nitride cantilever (ORC8, the typical tip radius of curvature was 15 nm; the spring constant was 0.05 N/m, Veeco). After AFM imaging, the film was rinsed overnight in an aqueous solution of 1 wt % sodium dodecyl sulfate to remove TMV from the film surface and was observed by AFM again.

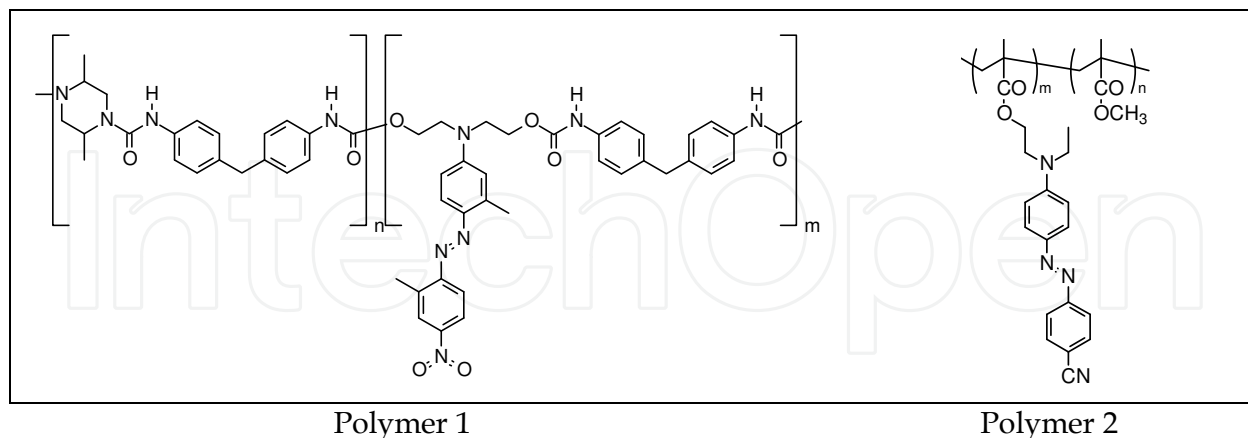


Fig. 5. Chemical structures of azopolymers in this study.

2.2.2 λ -DNA

λ -DNA as fibrous biomolecules is demonstrated to be immobilized on the azopolymer surface. The fibrous object in Fig. 6a is considered to be a bundle of λ -DNA (the diameter of the bundle is about 50 nm), which has been immobilized on the azopolymer surface by

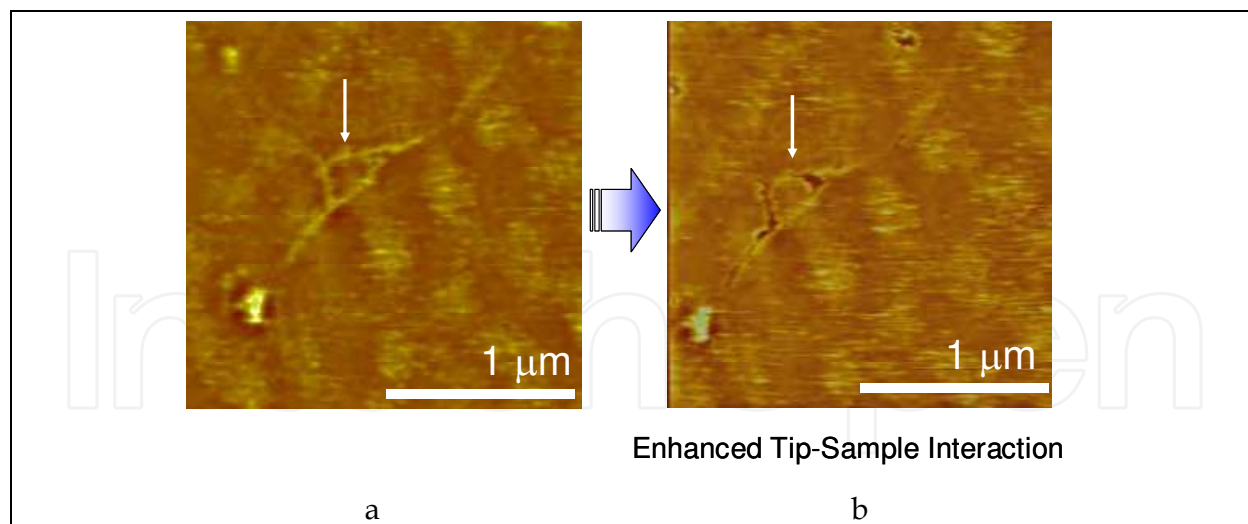


Fig. 6. The surface deformation on the azopolymer with DNA. a and b are contact-mode AFM images of the polymer surface covered with λ -DNA (The image height is from 0 to 20 nm). a, First scan of the surface covered with λ -DNA. b, the same image taken with a higher contact force after the first scan.

spin-casting from the DNA aqueous solutions and subsequent photoirradiation with laser light. By increasing the applied force of the AFM tip (Fig. 6b), the fibrous object is wiped away by the tip and it can be seen that the shape of the fibrous object is clearly imprinted as a fibrous valley on the azopolymer.

2.2.3 Immunoglobulin G

The globular biomolecules also can be immobilized on the azopolymer. Fig. 7 is AFM images of the IgG immobilized on the azopolymer surface. In Fig. 7a the azopolymer surface is covered with a layer of small granulated particles with 10 to 30 nm in diameter and around 8 nm in height (The height was estimated from the defects and the edge of the layer. Red markers in Fig. 7a.). The sizes of the particles are nearly equivalent to one subunit of IgG (about 10 nm, Fig. 1), considering the image includes the AFM tip-convolution artifact. The layer is so flat that the IgG monolayer is believed to be formed on the azopolymer surface. Fig. 7b shows an AFM image of the same area after washing the surface with PBS containing 2 wt% of SDS to remove the IgG layer. The dents of about 20 nm in diameter and 2 nm in depth are observed on the surface (a typical example is indicated by green markers in Fig. 7b, cross-section. Larger dents are also observed (red markers)). In contrast, as shown in Fig. 7c, no dents are formed on the azopolymer surface where no IgG was deposited. Comparing these images and cross sections, the dents formed on the azopolymer surface in Fig. 7b is considered to be mirroring the surface shape of the IgG layer shown in Fig. 7a.

Next, the retention of IgG on the azopolymer surface was investigated. Fig. 8a shows how the retention of fluorophore (Cy5)-linked IgG on the azobenzene-containing polymer surface changes with the photoirradiation time. The residual amount of IgG increases with the photoirradiation time and saturates over 30 min of photoirradiation. This time-dependent behavior is analogous to the polymer surface deformation; the deformation is increased with the photoirradiation time but is inclined to saturate. To investigate this

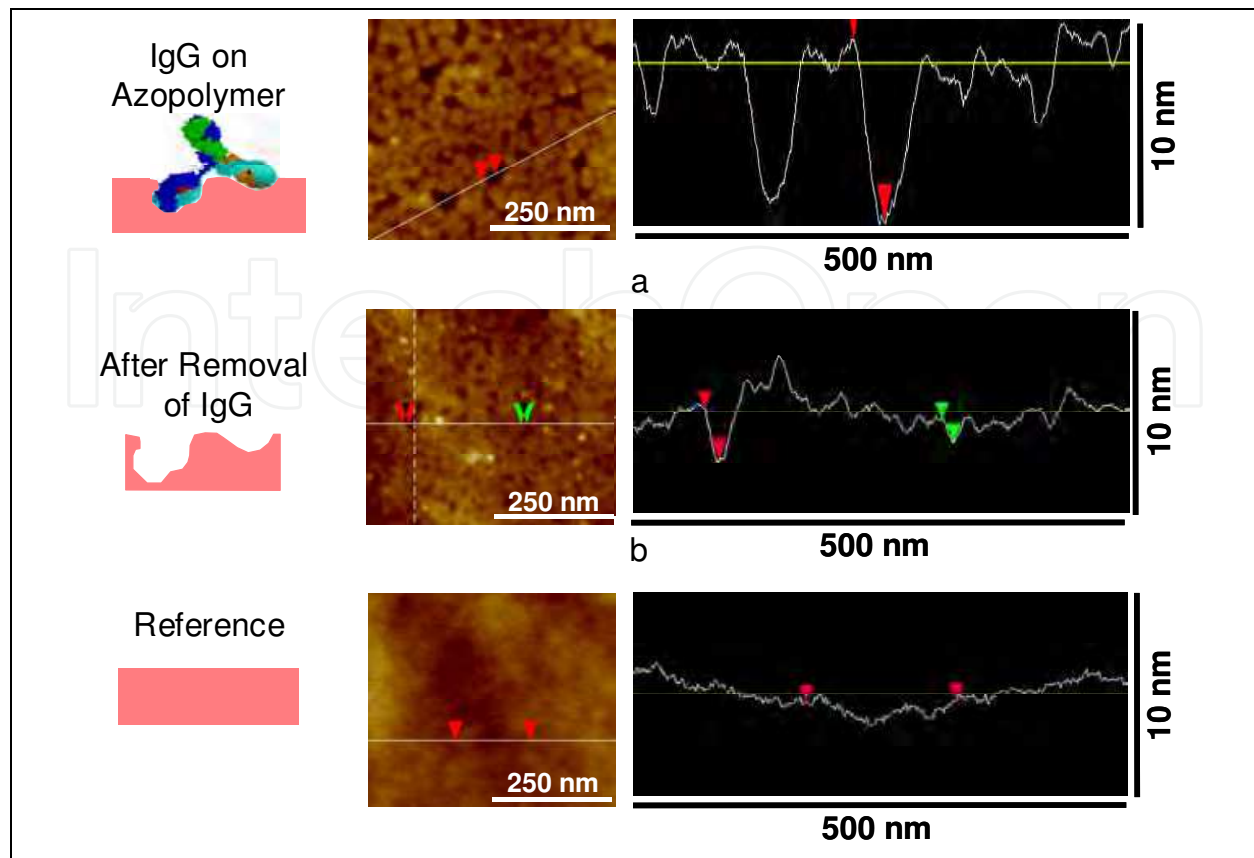


Fig. 7. The surface deformation on the azopolymer with IgG. a, A tapping-mode AFM image of the polymer surface covered with IgG. b, The same image taken after removal of the IgG by washing with PBS containing 2 wt% SDS. c, A control showing the bare azopolymer surface after photoirradiation. This image was taken at the outside of the above IgG spot.

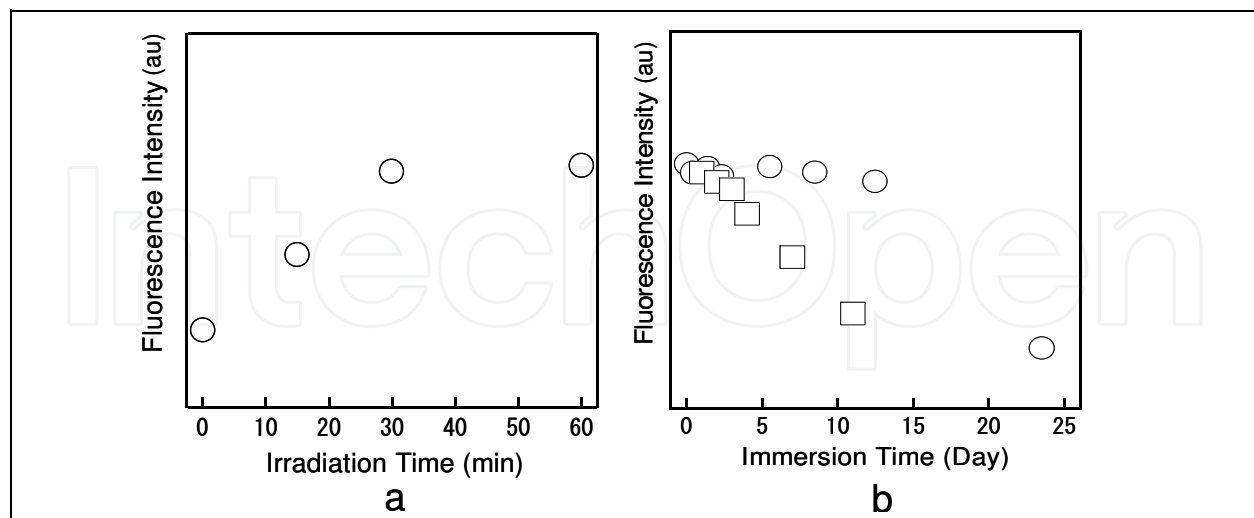


Fig. 8. The retention of fluorophore (Cy5)-linked IgG on the azopolymer surface after the photoirradiation. a, Photoirradiation time dependence of residual amounts of Cy5-linked IgG on the polymer. b, Desorption of IgG from the polymer surface in PBS after 30 min photoirradiation. Circles and squares denote results for 4 °C and room temperature, respectively.

desorption behavior further, the IgG-modified polymer surface which was photoirradiated for 30 min was soaked in PBS at room temperature and 4 °C (Fig. 8b). The IgG molecules immobilized on the polymer surface desorb very slowly on a time scale of several days, in contrast to a time scale of tens of minutes for the IgG molecules with the shorter photoirradiation time. Note that IgG molecules can be removed by just soaking in water. This suggests that the IgG molecules are physically, not chemically, immobilized on the polymer surface.

Activities of immobilized proteins, IgG on the azopolymer were investigated as follows. The temporal stability of the IgG activity was shown in Fig. 9. In Fig. 9a, the fluorescent IgG is immobilized on the lines of the spots A and B as controls, and the non-fluorescent IgG is immobilized on the lines of the spots C and D, and the spots has been reacted to the fluorescent antigenic IgG. The fluorescence intensity of the spots C and D are about 40 % of the intensity of the spots A and B. This means that 40% of the immobilized IgG is capable of capturing the antigens in solutions. Considering the steric hindrance between the IgG molecules, the activity of the immobilized IgG is very high. The immobilized IgG has been kept functioning very well for at least 6 months by the storage at 4 °C (Fig. 9). In the same way dozens of antibodies has been confirmed to continue to exhibit reactivity to specific antigens after immobilization on azopolymer.

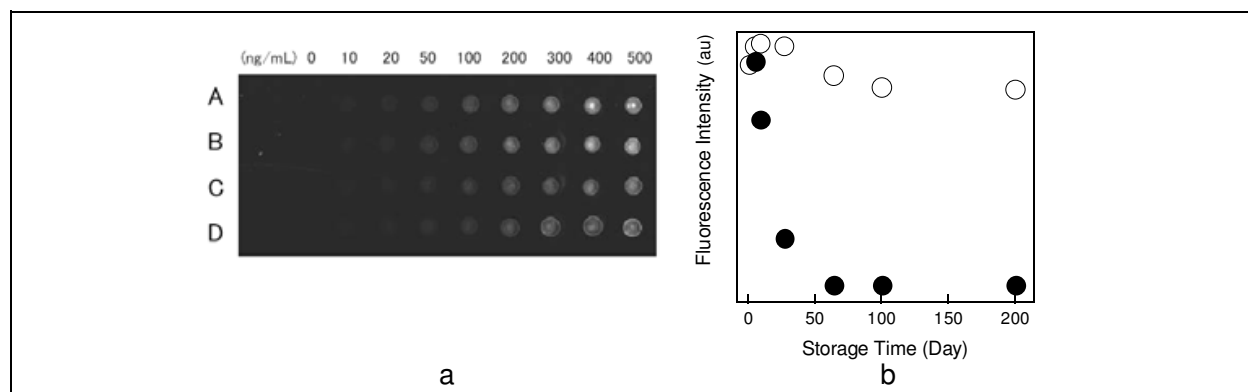


Fig. 9. The immunological activity of IgG immobilized on the azobenzene-containing polymer surface. a, A fluorescence image of the IgG spots (Cy5-linked Rabbit IgG was immobilized on A and B as controls, and Goat IgG to Rabbit IgG(H+L) was on C and D. The spot C and D had been reacted to Cy5-linked Rabbit IgG in the aqueous solution. b, The temporal stability of the IgG activity. Hollow and solid circles denote results for storage at 4 °C and at room temperature on dry condition, respectively.

2.2.4 Tobacco mosaic viruses

Fig. 10 shows contact-mode AFM images of the azopolymer surface treated with TMV. Shown in Fig. 10 a-c are the images of the sample in the presence of TMV for different photoirradiation times of 0, 10, and 20 min, respectively. All images show rod-shaped particles with a typical length of around 300 nm; however, the rods are not of uniform length. Some rods are shorter than 300 nm, and some are connected at each end. Several aggregations of granular particles are also observed in Fig. 10c. The granular particles on Fig. 10c were also observed on the samples of which preparation conditions were the same with Fig. 10a,b. Frequency of the appearance of the granular particles depended on the

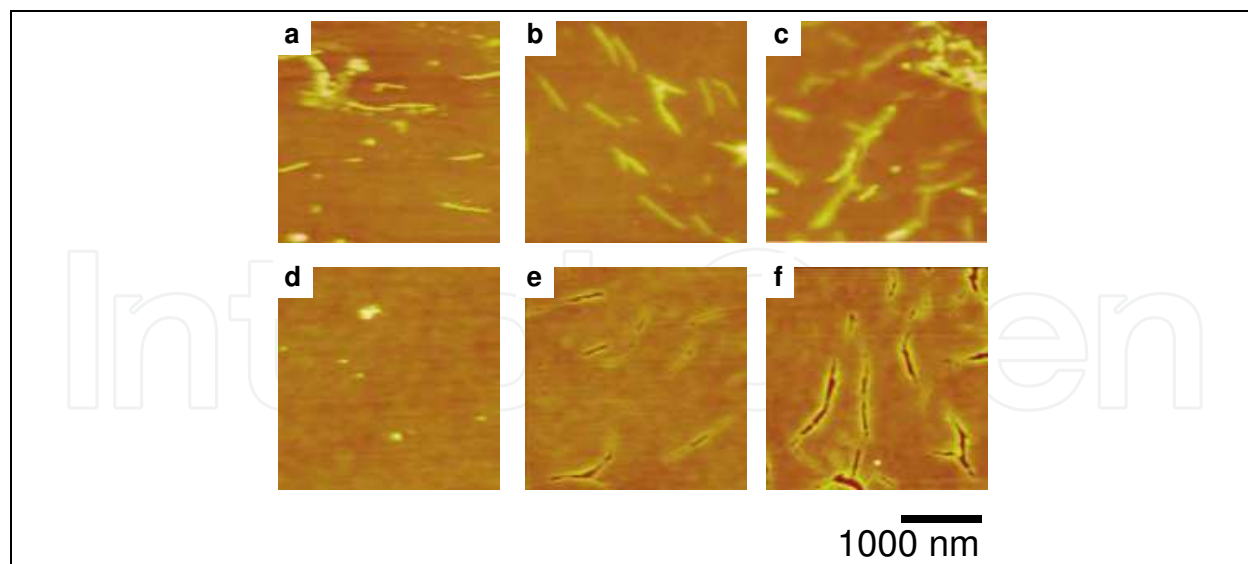


Fig. 10. AFM images of the azopolymer surface: (a–c) azopolymer surface in the presence of TMV; (d–f) azopolymer surface after washing the surface by detergent. (a, d) Without photoirradiation, (b, e) 10 min photoirradiation, and (c, f) 20 min photoirradiation.

sample preservation time; the frequency increased with increasing the preservation time after purification of the TMV stock solution. The granular particles were, therefore, not formed by the photoirradiation but formed during the preservation. These structures coincide with the structure seen by electron microscopy; the rods and the granular particles are attributed to TMV and decomposed materials from TMV (Casper, 1963; Shenton, 1999; Schramm, 1951).

Comparing Fig. 10a with Fig. 10b and Fig. 10c, strong image noises appear, and most of the rod-shaped particles are aligned parallel to the horizontal scanning direction in Fig. 10a. This strongly suggests that the rod-shaped particles on the surface are moved and aligned by the probe tip during scanning due to the unstable adsorption of TMV on the azopolymer surface. On the other hand, clear images of the rod-shaped particle are obtained in Fig. 10b,c. The heights of the rod-shaped particles gradually decrease with the photoirradiation time (Fig. 11a). This suggests that the rod-shaped particles are embedded into the azopolymer surface during the photoirradiation; therefore, the rods are immobilized firmly against the scanning of the probe tip. It must be noted that most of the rod-shaped particles are located in diagonal directions in Figure 10b. This is not due to the scanning of the probe tip, but rather to the flow of the buffer solution during the sample preparation, because the direction of the particles is different at each position even on the same sample. The TMV particles might be aligned along the convection flow during evaporating the solvent; for example, the convection flow was along the diagonal direction during the sample preparation in Fig. 10b.

Shown in Fig. 10d–f are contact-mode AFM images of the azopolymer surface after removal of TMV by washing with detergents; the samples were fabricated for different photoirradiation times of 0, 10, and 20 min, respectively. The flat surface with some small debris is observed in Fig. 10d. No deformation is caused on the azopolymer surface without photoirradiation. On the other hand, the observed structure of the grooves in Fig. 10e,f complements that of the rodlike particles shown in Fig. 10b,c, indicating that TMV shape is imprinted on the azopolymer surface by the photoirradiation.

Fig. 11 represents a detailed AFM analysis of the rod-shaped particles and the grooves on the azopolymer. The lateral and longitudinal cross sections of the typical rod-shaped particles on the azopolymer surface are shown in Figure 11a,b. From these cross sections, the rod-shaped particles are found to lay flat on the azopolymer surface, and the particles are gradually embedded while keeping their sides parallel to the azopolymer surface during the photoirradiation. Figure 11c shows a change in the average height of the rod-shaped particles as a function of the photoirradiation time. The height shown in the inset in Fig. 11c is averaged from 100 particles in several AFM images of the same sample. The average height decreases from 12 to 5 nm as the photoirradiation time increases from 0 to 30 min.

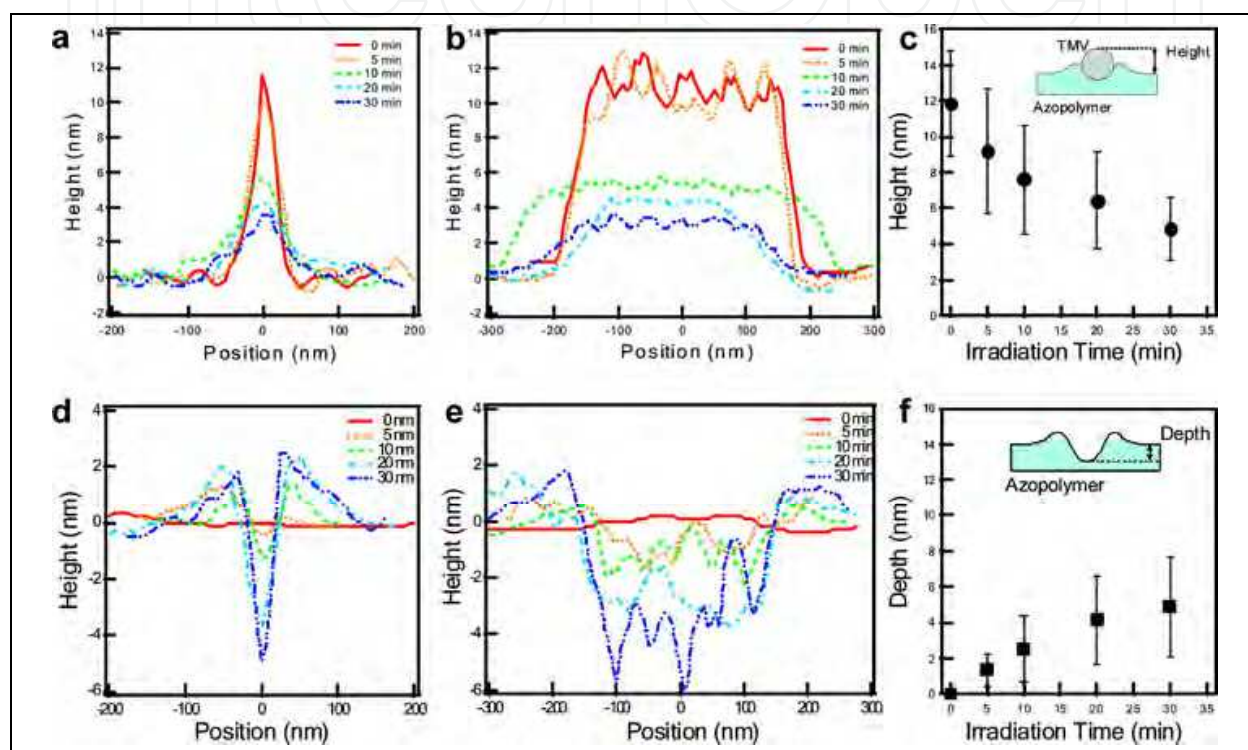


Fig. 11. AFM analysis of TMV on the azopolymer surface. (a, b) Cross sections of TMV on the azopolymer surface along with (a) lateral and (b) longitudinal directions. (c) Change in the height of the surface object on the azopolymer as a function of the photoirradiation time. The error bars indicate the standard deviations. (d, e) Cross sections of the grooves formed on the azopolymer surface after removal of TMV along with (d) lateral and (e) longitudinal directions. (f) Change in the depth of the groove formed on the azopolymer surface as a function of the photoirradiation time. The error bars indicate the standard deviations.

In the lateral cross sections in Fig. 11a, the full width at half-maxima (fwhm) of the peaks are around 30 nm, which is twice as large as the 18 nm diameter of TMV. This is due to the common imaging artifacts from a convolution of the probe geometry and the samples. Likewise, the average height at 0 min photoirradiation is 12 nm in Fig. 11c, which is smaller than the TMV diameter of 18 nm. This must be due to the strong interaction between the probe tip and TMV by the contact mode AFM operation, together with the unstable adsorption of TMV during the scanning in the AFM operation as shown in Fig. 10a. Although the cross sections contain these artifacts, it is evident that the height of the particles gradually decreases on a time scale of minutes during the photoirradiation.

The lateral and longitudinal cross sections of the typical grooves on the azopolymer surface after removal of the rod-shaped particles are shown in Fig. 11d,e. The lateral cross sections in Figure 11d show that the depth of the groove increases with the photoirradiation time accompanied by an uplift of the rim of the groove. The distance between the peaks of the rim is around 50 nm, which is 3 times larger than the diameter of TMV. The observed distance between the rims is accurate because the geometry of the sample surface, rather than of the probe, establishes the line profile of the peaks of the groove. On the other hand, the depth of the groove possibly appears small due to the probe tip not reaching the bottom of the groove. A change in the average depth of the grooves formed on the azopolymer surface as a function of the photoirradiation time is shown in Fig. 11f. The depth, defined in the inset in Fig. 11f, is averaged from 100 grooves in several AFM images of the same sample. By increasing the photoirradiation time to 30 min, the average depth of the grooves was increased to 5 nm. Sums of the average height in Figure 11c and the average depth in Figure 11f at the same photoirradiation time are kept constant at around 10 nm, which is smaller than the 18 nm diameter of TMV. The groove depth might be slightly underestimated due to the probe tip not reaching the bottom of the groove.

Based on the AFM analysis, the behavior of the azopolymer surface with TMV during the photoirradiation is summarized. As the photoirradiation time increases, TMV gradually embeds into the azopolymer surface because of the formation of the complement groove just beneath TMV. The groove depth increases with the uplift of the groove rim during the photoirradiation, but the distance between the groove rims stays constant at around 50 nm, 3 times larger than the diameter of TMV. To be precise, the geometry of the grooves on the azopolymer surface is slightly different from that of TMV. Finally, over half of the TMV body embeds into the groove after 30 min of photoirradiation. Overall, these results indicate that both the azopolymer surface deform along the shape of TMV during the photoirradiation. As a result, the contact-mode scanning of the probe tip in the AFM operations supports TMV in the groove formed on the azopolymer surface.

3. AFM imaging of supramolecular assemblies on the azopolymer

3.1 Supramolecular assemblies of actin filament

In this section, a structural study of supramolecular assemblies of cytoskeletal filamentous (F-) actin in the presence of divalent cation is presented (Ikawa et al., 2007). F-actin is a double-stranded helical filament made of the protein G-actin, can be considered as a semi-flexible and highly charged polyelectrolyte, with diameter $D_A \sim 80 \text{ \AA}$, persistence length $\xi_A \sim 10 \text{ \mu m}$ and anionic linear charge density $\lambda_A \sim -e/2.5 \text{ \AA}$. (Egelman, 2004; Wong et al., 2003) *In vitro*, F-actin in the presence of divalent cations assembles into gel-like networks and bundles that resemble their cellular counterparts formed with linker proteins. The F-actin/divalent cation aggregation has been used as a good model system, both experimentally and theoretically, for studying biological polyelectrolyte association. Recent experiments using high resolution small-angle X-ray scattering (SAXS) showed that with high concentration of divalent cations, F-actin forms bundles consisting of filaments that are closely packed in a distorted hexagonal arrangement. (Egelman, 2004; Wong et al., 2003) Within a small range in the low cation concentration regime, a unique layered structure consisting of stacks of nematic F-actin rafts was observed. The detailed structural phase behaviour of the F-actin supramolecular assembly challenges present theoretical model in many aspects. (Borukhov and Bruinsma 2001; Ha &

Liu, 1997; Lee et al., 2004) Clearly, in addition to the average structures revealed by XRD, to have a detailed view of the individual structural elements (filaments, bundles and networks) at the molecular level would provide much insight into the interactions that drive the self-assembly process of biological polyelectrolytes.

The AFM imaging technique based on the azopolymer was used to investigate the phase behaviour of F-actin aggregates as a function of concentration of the divalent cation Mg^{2+} . The data provided direct experimental evidence of a coil-on-coil (braided) structure of F-actin bundles formed at high Mg^{2+} concentrations. At intermediate Mg^{2+} concentrations, the data showed the first images of the two dimensional nematic rafts discovered by recent x-ray studies (Wong et al., 2003) and theoretical treatments. (Borukhov & Bruinsma, 2001)

3.1.1 Experimental procedure

F-actin was polymerized from lyophilized monomeric Globular (G-) actin (2mg/ml) from rabbit skeletal muscle. (Wong et al., 2003) F-actin length was controlled by the addition of an appropriate amount of 1 mg/mL gelsolin. The photoimmobilization process used to prepare the F-actin/ Mg^{2+} samples is as follows. F-actin and magnesium chloride solutions are spotted (each spot contains 1 μ L of $MgCl_2$ and 1 μ L of F-actin) and mixed on the surface of a spin-coated azopolymer film (polymer 2), on a glass substrate. Each sample (substrate) contains an array of spots (typically 6-8) with different concentrations of F-actin and Mg^{2+} . The film was then sealed inside a humidity chamber to prevent evaporation and irradiated for 60 minutes with light (470 nm) from a 6×10 array of blue light emitting diodes (LED) with an optical power density of 10 mW/cm². After washing the surface to remove excess sample, the substrate was probed by using a Digital Instruments Dimension 30000 scanning probe microscope in tapping-mode with a standard silicon cantilever (tip radius of curvature \sim 20 nm).

3.1.2 AFM image of F-actin filament and its assembly

An AFM image and an axial height trace of a single F-actin filament immobilized on the azopolymer surface is shown in Fig. 12. The height trace shows periodic variation with a typical repeating distance of 35 nm matching the pitch of the F-actin. The observed pitch varies from 30 nm to 40 nm, which is consistent with previous electron microscopy observations that F-actin is a helix with a random variable twist (Egelman, 2004; Egelman et al., 1982). The observed height (3 nm – 4 nm from valley to peak) of the filament is about half of the actual F-actin diameter (6-8 nm), suggesting that the filament is about halfway embedded into the azopolymer film after photoirradiation. The typical observed width of a single filament measured perpendicular to the filament is around 20 nm, about 3 times greater than the actual diameter of F-actin, which can be attributed to a tip-sample convolution effect. Even though it is difficult to remove this tip-sample convolution effect, it is not difficult to differentiate between single filaments and bundles based on their apparent diameter.

Fig. 13a-c demonstrates the progressive association of long actin filaments (up to \sim 10 μ m in length, no gelsolin) with increasing Mg^{2+} concentration (0 mM, 10 mM, 80 mM, respectively) on the azopolymer surface. The F-actin solution with 0 mM Mg^{2+} exhibits an uncondensed isotropic phase (Fig. 13a), with filaments maintaining large distances and intersecting angles (\sim 90 degrees) between them to minimize electrostatic repulsion. With 10 mM Mg^{2+}

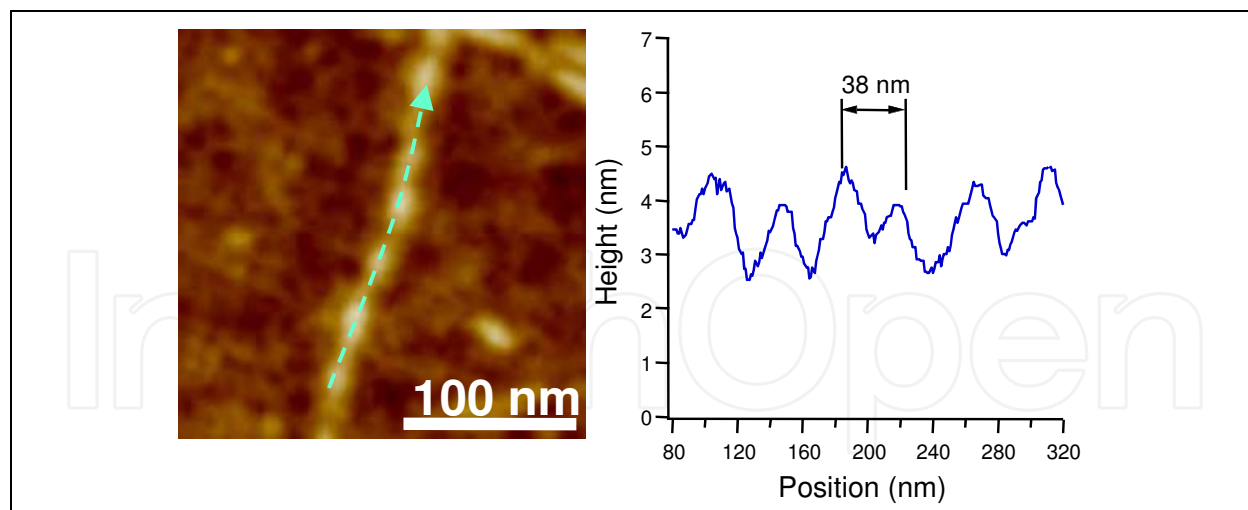


Fig. 12. An AFM image of a single F-actin filament and a height trace along the single filament showing periodic variations corresponding to F-actin twists.

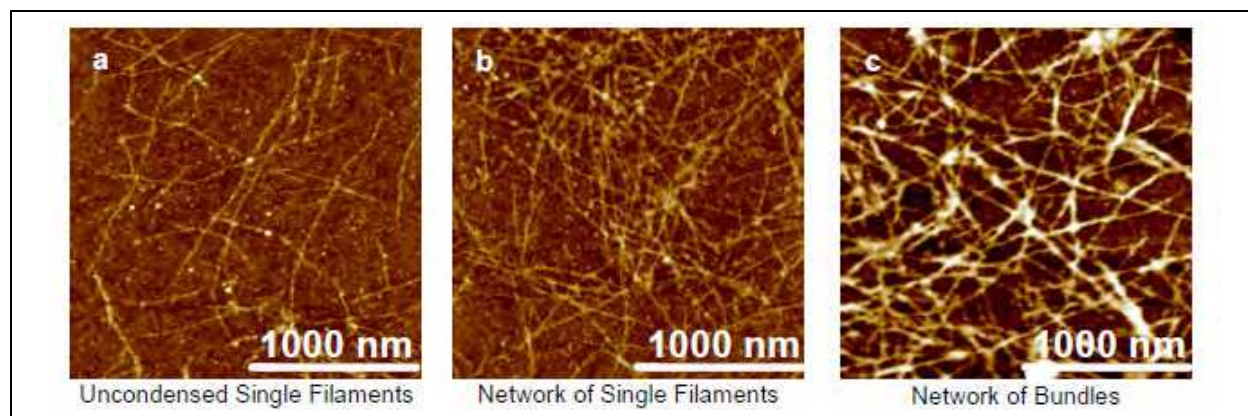


Fig. 13. AFM images showing the progressive association of long (no gelsolin) actin filaments as a function of Mg^{2+} concentration. (a) Isotropic phase of F-actin (0 mM Mg^{2+}). (b) Network of F-actin (10 mM Mg^{2+}). (c) Network of F-actin bundles (80 mM Mg^{2+}). The phase map was obtained from one azo-polymer sample containing multiple spots of F-actin/ Mg^{2+} mixed at different ratios.

(Fig.13b), the distances between filaments become smaller and the filaments form a network structure with smaller intersecting angles between filaments. The network consists of predominantly single filaments of F-actin. At 80 mM Mg^{2+} (Fig.13c), however, a different network structure composed of mostly thick filaments (F-actin bundles), is observed. The single filaments and bundles are entangled and oriented randomly in the network, suggesting little excluded volume interaction which drives liquid crystalline ordering in the more concentrated solution. Interestingly, the bundles observed in the networks appear to be fairly uniform in diameter and large bundles were rarely seen under this condition. This suggests that there might be a growth limit of the bundle size, which has been predicted theoretically. Overall, the phase behaviour observed in the AFM images is consistent with the previous results obtained using x-ray diffraction and optical microscopy. However, the high resolution data allowed us to examine the structures at a single filament or bundle level, which led to observations relevant to several important unanswered questions about F-actin assemblies.

There has been much discussion about the structure of bundles that are formed by charged biopolymers at high counter-ion concentrations. One of the intriguing possibilities is whether the F-actin could form helical coil within a bundle. (Shao et al., 2000) Analogous structures have been theoretically predicted, but never experimentally verified. Using the current technique, direct evidence of the coil-on-coil (braided) bundle structure at higher cation concentrations has been found (>20 mM Mg^{2+}). In Fig. 14a,b, two examples of the braided bundles formed with short F-actin (average length = 680 nm controlled with gelsolin) and 80 mM Mg^{2+} are shown. Under this condition, co-existence of both single filaments and bundles were observed, which can be easily differentiated in the magnified images by their apparent diameter. Following the trace lines, it can be seen that the bundles unravel at their ends into three or more single filaments. The braided configuration of the bundle is especially obvious in Fig. 14b. The braided structure is found to exist in a wide range of Mg^{2+} concentrations (5 mM to 160 mM), from the uncondensed phase to the bundled phase. In comparison, such spiral structures were not readily discernible in the bundles that are formed by longer filaments (Fig. 14c). One could argue that the longer filaments are more prone to kinetic hindrance to forming braided structures due to increased difficulty in rotational movements.

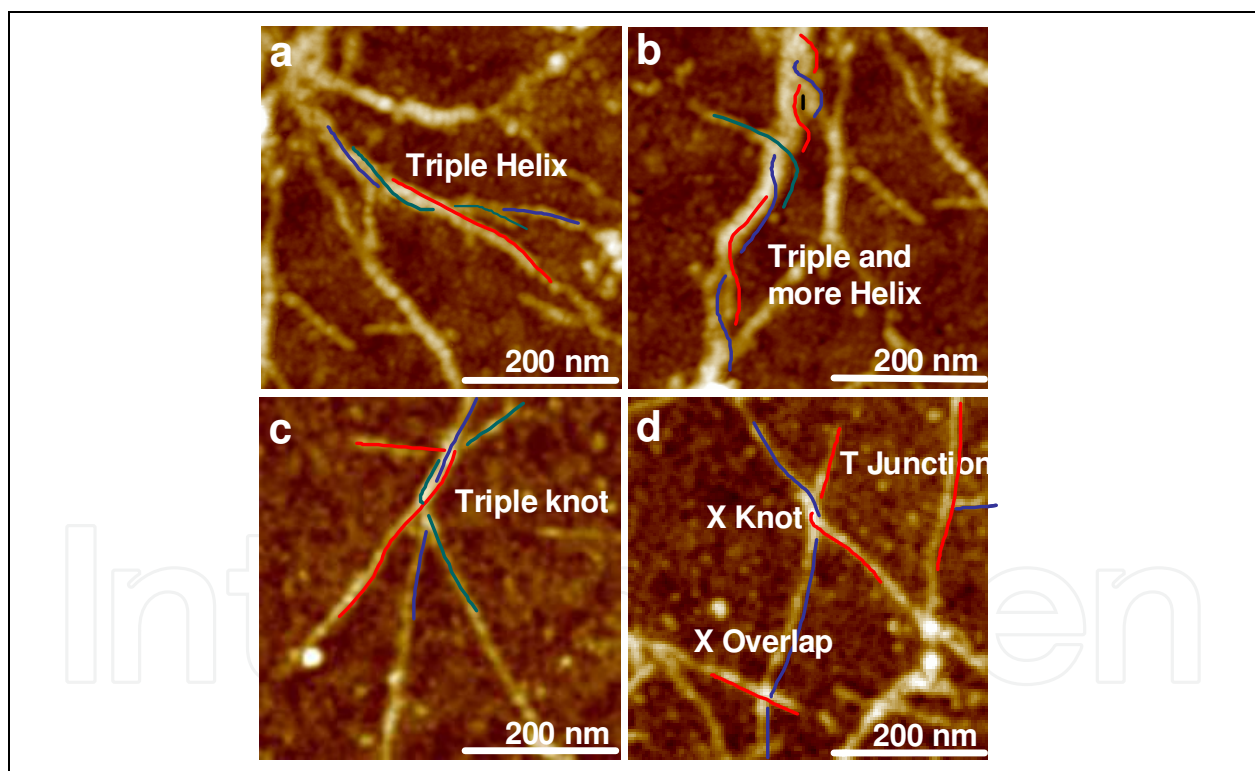


Fig. 14. Braided structures of short F-actin (average length 680 nm) bundles and precursor junctions. (a, b) Braided bundles at high concentration of Mg^{2+} (80 mM). The bundle in image (a) consists of three filaments and the bundle in (b) consists possibly of more than three filaments. (c, d) Junction-type precursor structures formed in the uncondensed phase of F-actin with 5 mM Mg^{2+} . All the images are 0-10 nm in height.

AFM images of F-actin at lower Mg^{2+} concentrations offered some clues as to how the helical bundles may be formed. Fig. 14c,d show several distinct F-actin junctions (points

where single filaments are joined or crossed) observed at 5 mM Mg^{2+} concentration. In Fig. 14c, three filaments form a knot structure of about 100 nm in length, and the knot unravels at both ends into three single filaments with fairly large angular separation. Also, entangled points formed by two filaments are observed in Fig. 14d. In the same image, two other types of joints could be seen: an X overlap in which the two filaments simply cross each other and a T junction where the end of one filament is seemingly attached to another filament at a near 90 degree angle. All these junctions can be considered as precursor sites of the more extensive helical bundle structure shown in Fig. 14a,b at higher Mg^{2+} concentrations.

The braided bundle structure may have been present in previous images of F-actin bundles obtained using electron microscopy, AFM, and confocal optical microscopy, but was not recognized as such. For example, high resolution cryo-AFM images of F-actin clearly showed the existence of braided bundles. (Shao et al., 2000) Synchrotron x-ray diffraction data showed that the close packing pattern of the bundle deviates from an exact hexagonal arrangement ($q_{10}=0.089\text{\AA}^{-1}$ and $q_{11} = 0.139\text{\AA}^{-1}$, respectively), which may be partially attributed to the braided arrangement of some F-actin inside the bundle. (Angelini, et al., 2003, Wong, et al. 2003) The observed axial repeat distance of the braided bundles is around 100 nm (Fig. 14b,c), comparable to the pitch of a single F-actin twisted structure. This strongly suggests that the F-actin filament follows the topology of the twist of F-actin in order to achieve tighter packing.

It is important to note that the existence of braided F-actin bundles does not necessarily contradict the earlier conclusion of hexagonal packing of filaments inside the bundles. Because of the limited statistical sampling of AFM imaging and the large F-actin length distribution, it is likely that the actual samples contain both structures, with hexagonal bundles being the prevalent structure giving rise to the x-ray diffraction peaks.

The structures formed in the intermediate range of concentration are of particular interests, as previous x-ray studies revealed in this regime an unique phase composed of lamellar stacks of crossed rafts (L_{XR} phase; Wong, et al. 2003). Such a structure, formed with 20 mM of Mg^{2+} , is shown in Fig. 15a. The filaments form a 2D nematic-like rafts with a lateral repeat distance of about 12 nm, slightly larger than the F-actin diameter. The rafts are stacked at a large angle from each other, as was deduced from x-ray data, which showed a series of strong (00L) harmonic peaks due to stacking. The raft-like structures can be observed in a wide range of Mg^{2+} concentration (5-40 mM) with short F-actin and were much less dominant with longer filaments. This is consistent with the phase diagram compiled with x-ray data. (Wong et al., 2003) Similar structure has been observed in the system consisting of microtubules and divalent cations, suggesting a certain degree of universality of phase behaviour of rod-like biological filaments with divalent cations.

The 2D nematic-like rafts were found to coexist with aggregated perpendicular filaments at slightly lower Mg^{2+} concentrations (5-10 mM), as shown in Fig. 15b, which is consistent with recent molecular dynamic simulation predictions that isolated stiff polyelectrolyte filaments in general evolve from aggregated perpendicular filaments to aggregated parallel rods.¹⁶ The theoretical treatment also describes that the aggregated perpendicular filaments can form two-dimensional rafts. (Borukhov et al., 2001) This image clearly shows the coexistence of the parallel filaments and the perpendicular one.

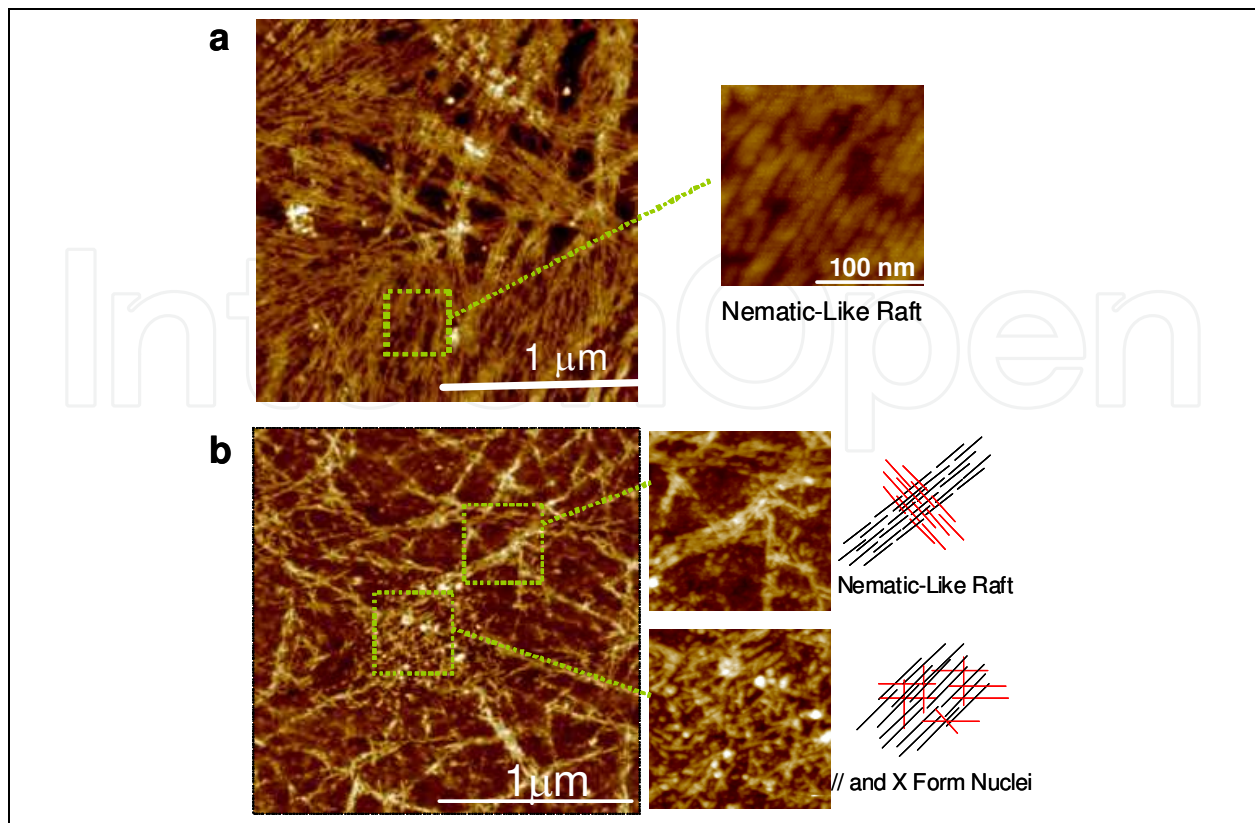


Fig. 15. AFM images of intermediate phases of short F-actin (average length 170 nm) Mg²⁺. (a) A phase consists of the nematic-like rafts with 20 mM Mg²⁺. In part, the rafts are stacked. (b) A phase consists of both the nematic-like rafts and the perpendicular aggregates with 10 mM Mg²⁺.

Based on the above AFM images, the phase diagram of the supramolecular assembly of F-actin was summarized in Fig. 16. The structures of the assemblies changes with concentration of Mg²⁺ and length of the filaments, which is consistent with the previous X-ray study and the theoretical predictions. (Borukhov et al., 2001; Wong et al, 2003) The AFM study clearly shows the first-time-seen images of the following structures: (1) the cross stacking of the 2D nematic-like rafts of short F-actin at intermediate concentration of Mg²⁺ (5 - 10 mM) and (2) the braided bundle structure at high concentration of Mg²⁺ (more than 20 mM).

3.2 AFM image of myosin filaments

Cytoskeletal motor proteins myosin associated with actin filament tracks through a head region, called motor domain, that binds and hydrolyzes ATP. The Myosin from muscle protein called Myosin II, which generates the force for muscle contraction. Myosin II is an elongated protein that is formed from two heavy chains and two copies of each of two light chains. Each of the heavy chains has a globular head chains at its N-terminus that contains the force-generating domain, followed by a very long amino acid sequence that forms an extended coiled-coil that mediates heavy chain dimerization. The two light chain bind close to the N-terminal head domain, while the long coiled-coile tail bundles itself with the tails of other myosin molecules. These tail-tail interaction *in vivo* results in the formation of larger bipolar thick filaments (Alberts et al., 2002).

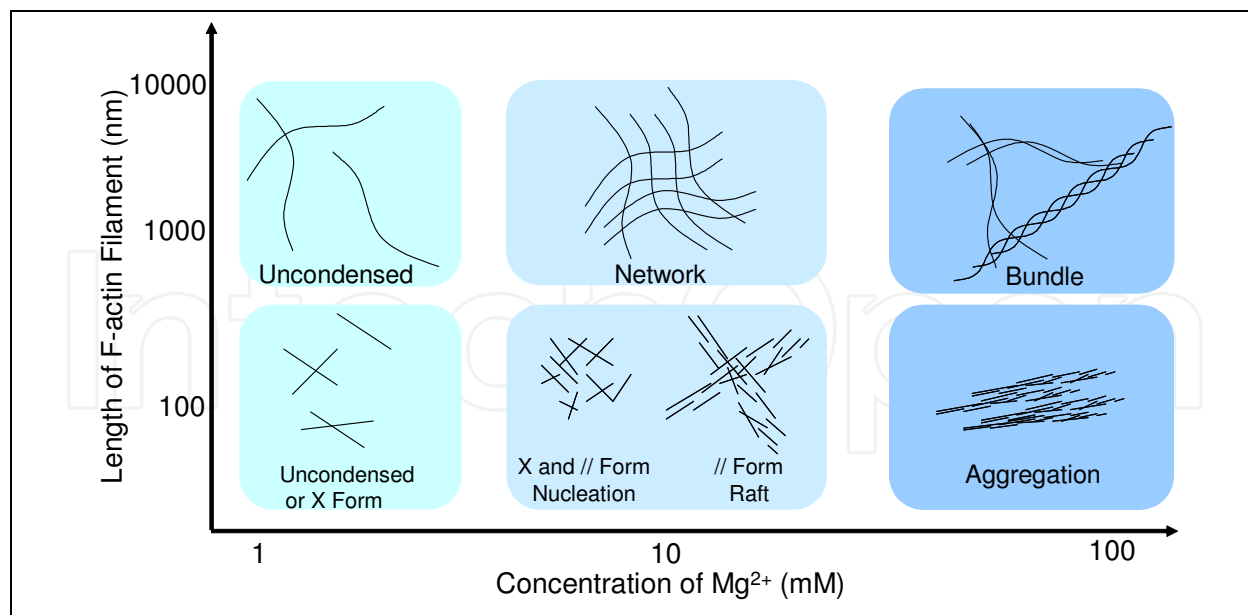


Fig. 16. A phase diagram of the supramolecular assembly of F-actin as a function of Mg^{2+} concentration.

The assembly of the myosin *in vitro* can be regulated by ionic strength and preparation condition (Offer, 1987). When the salt concentration of solution of myosin is reduced, either by dilution or by dialysis, the myosin molecules polymerize into filaments; the tendency for filament formation increases as either the salt concentration or pH is reduced. The structure of the synthetic filaments formed is not fixed but varies grossly with the final ionic condition and the rate at which the salt concentration is reduced.

The structure of the myosin filaments is analysed by AFM imaging using the azopolymer. Myosin from rabbit skeletal muscle (22 mg/ml containing 20 mM TES, pH7.0, 0.6 M NaCl, 50 % of glycerole, Prozyme) was diluted or dialyzed by aqueous buffer solution containing imidazole, potassium chloride, magnesium chloride. Final concentration of the buffer was summarized in Table 1. The photoimmobilization process used to prepare the myosin filament samples is as follows. The myosin filament solutions are spotted (each spot contains 1 μ L) on the surface of a spin-coated azopolymer film (polymer 2), on a glass substrate. The film was then sealed inside a humidity chamber to prevent evaporation and irradiated for 60 minutes with light (470 nm) from a 6x10 array of blue light emitting diodes (LED) with an optical power density of 25 mW/cm². After washing the surface to remove excess sample, the substrate was probed by using a Digital Instruments Nanoscope E scanning probe microscope in contact-mode with a standard silicon cantilever (tip radius of curvature ~ 20 nm).

sample	Concentration of Myosin (mg/mL)	pH	Buffer			Preparation Method	Filament Size	
			Imidazole (mM)	KCl (mM)	MgCl ₂ (mM)		Lentgh(nm)	Diameter(nm)
a	0.25	7.4	20	25	4	Dialysis	>10000	5 - 20
b	0.2	7.4	20	25	4	Dilution	>2000	5 - 10
c	0.77	7.4	20	25	160	Dilution	500	2 - 5
d	0.71	7.4	20	500	4	Dilution	200	2

Table 1. Preparation condition for AFM imaging of the myosin filament in Fig. 17.

Fig. 17 shows the AFM images of the myosin filaments immobilized on the azopolymer surface. Comparing Fig. 17a and b, the size of the filament is shown to be affected by the preparation condition. By dialysis, the filament became very large and entangled, on the other hand, the filament became smaller and uniform by dilution. When the ionic strength of the buffer became higher, the filaments changes to smaller and uniform size (Fig. 17b,c). These images clearly shows that the immobilization method does not affected by the buffer ionic condition.

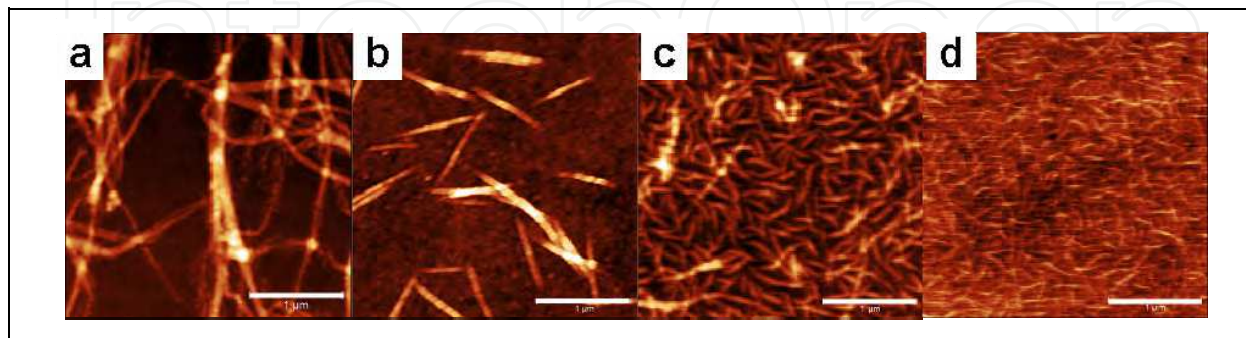


Fig. 17. AFM Images of Myosin Filaments immobilized on the Azopolymer surface. Scale bar 1000 nm. a, b, c and d corresponds in Table 1

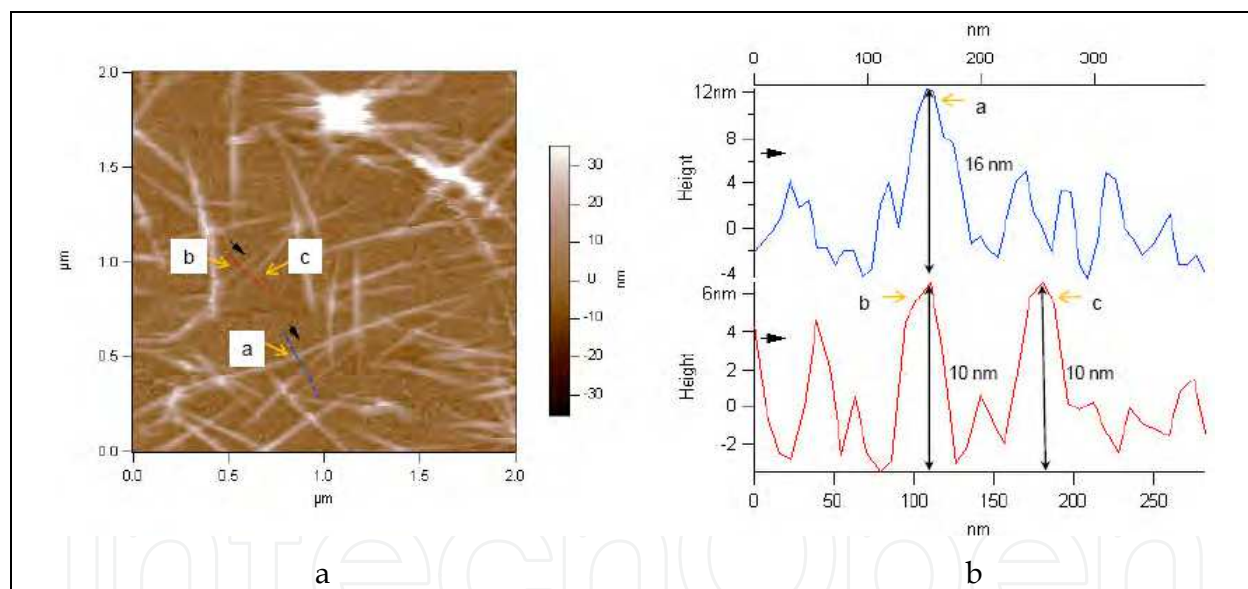


Fig. 18. AFM image of myosin filament obtained in fluid condition. 2-dimensional image (a) and the cross section (b).

The AFM imaging of myosin is also performed in fluid condition. After immobilizing the myosin in the buffer on the azopolymer by photoirradiation, the solution is rinsed by the same buffer. Immediately, the fluid imaging is performed by Asylum Research MFP-3D-BIO Atomic Force Microscope in tapping-mode.

Fig. 18 shows the AFM image of Myosin filament, the buffer condition is same as the sample b in Table 1 and Fig 18b. This image clearly shows that the myosin filaments are immobilized on the azopolymer surface even in the fluid condition and the filament size is almost the same as the one obtained even in air condition by contact-mode AFM, which is higher

sample-tip interaction. The experiments shows that the ionic strength is not affected by the immobilization on the azopolymer, and that the AFM images obtained both in fluid and air conditon are the essentially the same.

4. Conclusion

The immobilization technique using the azopolymer is well-suited for AFM imaging of biomolecules and their assembly because it can provide a non-reactive, non-ionic, and flat surface on which the complex supramolecular assemblies can be immobilized in the native aqueous environment, reducing the possibility of chemical denaturation of the immobilization objects. The immobilization process dramatically reduces the thermal motion of biomolecules, leading to higher imaging resolution allowing individual biomolecules to be resolved without interference from the substrate. Clear biomolecule images appeared on the azopolymer surface after the photoirradiation, even by using contact-mode AFM where interaction between the probe tip and the sample is relatively strong.

There is an important disadvantage when compared with atomically flat mica surface as a substrate for AFM imaging; the information about the height of the object is spoiled by its embedding into the azopolymer surface. However, comparing the observed height of the object with the groove formed on the azopolymer surface, the true height can be estimated. Another disadvantage is that the azopolymer used in this experiment is inadequate for the immobilization of highly charged objects like TMV in the aqueous condition. (Note that general hydrophilic proteins, for example IgG, green fluorescent protein, and F-actin, could be immobilized on the same azopolymer surface in aqueous media.). To immobilize highly charged objects like TMV in the aqueous condition, introduction of a counter charged functional group to the azopolymer is essential.

In summary the technique is of greater advantage than the conventional methods in points of versatility and simplicity for AFM imaging biomolecules and their assembly.

5. Acknowledgment

Author thanks C.R. Safinya, Youli Li, Kai Ewert, L.S. Hirst, N. Bouxsein, M.C. Choi and R. Beck for useful discussions. Author thanks Y. Kato, T. Yamada, M. Shiozawa, M. Narita, M. Mouri, F. Hoshino, T. Mitsuoka, T. Matsuyama, H. Takahashi, O. Watanabe and S. Ito for their kind support for this work. Author thanks H. Takami and H. Sugasawa of Asyrum Technology Co. Ltd for fluid imaging of myosin.

6. References

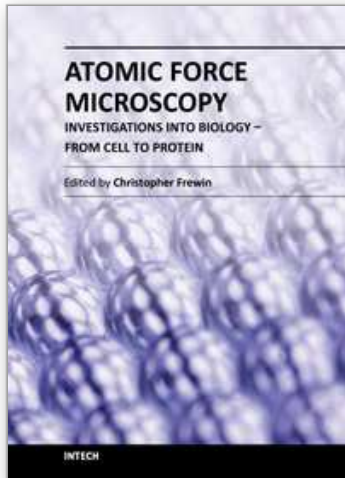
- Alberts, B.; Johnson, A.; Lewis, J., Rall, M.; Roberts, K. & Walter, P. (2002) Chapter 16, Molecular motors, In *Molecular Biology of the Cell 4th Ed.*, pp.949-952 Garland Science, New York, USA
- Alexander, C.; Davidson, L. & Hayes, W., (2003), Imprinted polymers: artificial molecular recognition materials with applications in synthesis and catalysis. *Tetrahedron*, Vol.59, pp.2025-2057

- Angelini, T.E.; Liang, H.; Wriggers, W. & Wong, G.C.L., (2003) Like-charge attraction between polyelectrolytes induced by counterion charge density waves, *Proc. Natl. Acad. Sci. USA*, Vol. 100, pp.8634-8637
- Bezanilla, M.; Manne, S.; Laney, D.E.; Lyubchenko, Y.L. & Hansma, H.G. (1995), Adsorption of DNA to mica, silylated mica and minerals: characterization by atomic force microscopy. *Langmuir*, vol. 11, pp.655-659
- Borukhov, I. & Bruinsma, R.F., (1997), Counterion-mediated attraction between two like-charged rods. *Phys. Rev. Lett.* vol.79, 1289-1292
- Borukhov, I. & Bruinsma, R. F., (2001) Raft instability of biopolymer gels. *Phys. Rev. Lett.* Vol.87, 158101
- Casper, D.L.D., Assembly and stability of the tobacco mosaic virus particle. *Adv. Protein Chem.* Vol.18, pp.37-121
- Curtis, A. & Wilkinson, C., (2001), Nanotechniques and approaches in biotechnology. *Trends in biotechnology*, Vol. 19, pp.97-101
- Cunin, F.; Schmedake, T.A.; Link, J.R.; Li, Y.Y.; Koh, J.; Bhatia, S. N. & Sailor, M. J. (2002) Biomolecular screening with encoded porous silicon photonic crystals. *Nature Materials*, Vol. 1, pp.39-41
- Egelman, E.H. (2004) Acrosomal actin: twists and turns of a versatile filament. *Curr. Biol.* Vol.14, R959
- Egelman, E. H., Francis, N., DeRosier, D. J., (1982), F-actin is a helix with a random variable twist. *Nature*, Vol. 298, pp. 131-135
- Ha, B.-Y. & Liu, J. A., (1997), Counterion-mediated attraction between two like-charged rods. *Phys. Rev. Lett.*, Vol.79, pp.1289-1292
- Hansma, H.G., (2001) Surface biology of DNA by atomic force microscopy. *Annual Rev. Phys. Chem.*, Vol.52, pp.71-92
- Hasegawa, M.; Ikawa, T.; Tsuchimori, M.; Watanabe, O.; Kawata, Y., (2001) Topographical nanostructure patterning on the surface of a thin film of polyurethane containing azobenzene moiety using the optical near field around polystyrene spheres. *Macromolecules*, Vol.34, pp.7471-7476
- Haupt, K.,(2003) Imprinted polymers - Taylor-made mimics of antibodies and receptors. *Chem. Comm.* pp.171-178.
- Ichimura, K., (2000) Photoalignment of liquid-crystal systems. *Chem. Rev.*, Vol.100, 1847
- Ikawa, T.; Hoshino, F.; Matsuyama, T.; Takahashi, H. & Watanabe, O., (2006), Molecular-shape imprinting and immobilization of biomolecules on a polymer containing azo dye, *Langmuir*, Vol.22, No.6, pp.2747-2753
- Ikawa, T.; Hoshino, F.; Watanabe, O.; Li, Y.; Pincus, P. & Safinya, C.R., (2007), Molecular-scale imaging of F-actin assemblies immobilized on a photopolymer surface, *Phys. Rev. Lett.*, Vol.98, 018101
- Ikawa, T.; Kato, Y.; Yamada, T.; Shiozawa, M.; Narita, M.; Mouri, M.; Hoshino, F.; Osamu, W.; Tawata, M. & Shimoyama, H., (2010), Virus-templated photoimprint on the surface of an azobenzene-containing polymer, *Langmuir*, Vol.26, No.15, pp.12673-12679
- Ikawa, T.; Mitsuoka, T.; Hasegawa, M.; Tsuchimori, M.; Watanabe, O.; Kawata, Y.; Egami, C.; Sugihara, O.; Okamoto, N. (2000) Optical near field induced change in viscoelasticity on an azobenzene-containing polymer surface. *J. Phys. Chem., B.* Vol.104, pp 9055-9058

- Ikawa, T.; Mitsuoka, T.; Hasegawa, M.; Tsuchimori, M.; Watanabe, O. & Kawata, Y., (2001) Azobenzene polymer surface deformation due to the gradient force of the optical near field of monodispersed polystyrene spheres. *Phys. Rev. B.*, Vol. 64, 195408
- Kambhampati, D., (Ed.) , (2003), In: *Protein Microarray Technology*, Wiley-VCH, Weinheim, Germany
- Karageogiev, P.; Neher, D.; Schulz, B.; Stiller, B.; Pietsch, U.; Giersig, M. & Brehmer, L. (2005) From anisotropic photo-fluidity towards nanomanipulation in the optical near-field, *Nature Mater.* Vol.4, pp.699-703
- Kawata, Y.; Egami, O.; Nakamura, O.; Sugihara, M.; Okamoto, M.; Tsuchimori, M. & Watanabe, O., (1999) Non-optically probing near-field microscopy, *Opt. Commun.* Vol.161, pp.6
- Kim, D.Y.; Li, L.;Kumar, J. & Tripathy, S.K.,(1995) Laser-induced holographic surface relief gratings on nonlinear optical polymer films, *Appl. Phys. Lett.* Vol.66, pp.1166-1168
- Lamtore, J.B.; Beattie, K.L.; Burke, B.E.; Eggers, M.D.; Ehrlich, D.J.; Fowler, R.; Hollies, M.A.; Kosicki, B.B.; Reich, R.K.; Smith, S.R.; Varma, R.S. & Hogan, M.E., (1994) Direct detection of nucleic acid hybridization on the surface of a charge coupled device, *Nucleic Acids Res.*, Vol. 22, pp. 2121
- Lee, K-C.; Borukhov, I.; Gelbart, W. M.; Liu, A.J.; Stevens, M. J. ,(2004), Effect of mono- and multivalent salts on angle-dependent attractions between charged rods. *Phys. Rev. Lett.* Vol. 93, 128101
- Mayers, A. G., (2002), In: *Biomolecular Sensors*, Gizeli, E., Lowe, R. C., (Eds), Taylor and Francis, London, England
- Mouri, M.; Ikawa, T.; Narita, M.; Hoshino, F. & Watanabe, O., (2010) Orientation Control of Photo-Immobilized Antibodies on the Surface of Azobenzene-Containing Polymers by the Introduction of Functional Groups, *Macromol, Biosci.*, Vol. 10, pp.612
- Natanshon, A. & Rochon, P., (2002) Photoinduced motions in azo-containing polymers, *Chem. Rev.*, Vol.102, pp. 4139
- Offer, G. (1987), Chapter 12 Myosin filaments, In *Fibrous Protein Structure*, PP.307-356, Academic Press, N
- Ostuni, E.; Chapman, R. G.; Holmlin, R. E.; Takayama, S. & G. M. Whitesides, (2001) A survey of structure-property relationships of surfaces that resist the adsorption of protein, *Langmuir*, Vol.17, pp.5605-5620
- Ramsden, J. J., (1993) Experimental methods for investigating protein adsorption kinetics at surfaces, *Quarterly Reviews of Biophysics*, Vol.27, pp.41-105
- Rau, H.; (1990), In *Photochemistry and Photophysics*, J. K. Rabek, (Ed.), CRC Press: Boca Raton, Flance, Vol. 2, pp.119-121.
- Rochon, P.; Batalla, E. & Natansohn, A., (1995) Optically induced surface gratings on azoaromatic polymer films, *Appl. Phys. Lett.* Vol.66, pp.136-138
- Schena, M., (Ed.), (2004), In: *Protein Microarray*, Jones and Bartlett Publishers, Sudbury, USA.
- Schramm, G. & Wiedeman, M.,(1951) , *Z. Naturforsch. B*, Vol. 6, 379
- Shao, Z.; Shi, D. & Somlyo A.V. (2000), Cryoatomic force microscopy of filamentous actin, *Biophys. J.*, Vol. 78, pp. 950-958
- Shenton, W.; Douglass, T.; Young, M.; Stubbs, G.; Mann, S. (1999) Inorganic-organic nanotube composites from template mineralization of tobacco mosaic virus, *Adv. Mater.*, Vol.11, pp.253-256

- Shi, H.; Tsai, W-B.; Garrison, M.D.; Ferrari, S. & Ratner, B. D., (1999) Template-imprinted nanostructured surfaces for protein recognition, *Nature*, Vol.398, pp.593-597
- Todorov, T.; Nikolova, L., Tomova, N., (1984) Polarization holography. 1: A new high-efficiency organic material with reversible photoinduced birefringence, *Appl. Opt.* Vol. 23, pp. 4309-4312
- Wahlgren, M. & Arnebrant, T., (1991) Protein adsorption to solid surfaces., *TIBTECH*, Vol.9, pp.201-208.
- Watanabe, O.; Ikawa, T.; Kato, T.; Tawata, M. & Shimoyama, H. (2006) Area-selective photoimmobilization of a two-dimensional array of colloidal spheres on a photodeformed template formed in photoresponsive azopolymer film, *Applied Physics Letters*, Vol. 88, 204107-204109
- Wong, G.C.L.; Lin, A.; Tang, J.X.; Li, Y.; Janmey, P.A. & Safinya, C.R., (2003) Structure of actin cross-linked with alpha-actinin: A network of bundles, *Phys. Rev. Lett.*, Vol.91, 08103.
- Whitesides, G. M.; Ostuni, E.; Takayama, S.; Jiang, X. & Ingber, D. E. (2001) Soft Lithography In Biology And Biochemistry, *Annu. Rev. Biomed. Eng.* Vol. 3, pp. 335-373.

IntechOpen



Atomic Force Microscopy Investigations into Biology - From Cell to Protein

Edited by Dr. Christopher Frewin

ISBN 978-953-51-0114-7

Hard cover, 354 pages

Publisher InTech

Published online 07, March, 2012

Published in print edition March, 2012

The atomic force microscope (AFM) has become one of the leading nanoscale measurement techniques for materials science since its creation in the 1980's, but has been gaining popularity in a seemingly unrelated field of science: biology. The AFM naturally lends itself to investigating the topological surfaces of biological objects, from whole cells to protein particulates, and can also be used to determine physical properties such as Young's modulus, stiffness, molecular bond strength, surface friction, and many more. One of the most important reasons for the rise of biological AFM is that you can measure materials within a physiologically relevant environment (i.e. liquids). This book is a collection of works beginning with an introduction to the AFM along with techniques and methods of sample preparation. Then the book displays current research covering subjects ranging from nano-particulates, proteins, DNA, viruses, cellular structures, and the characterization of living cells.

How to reference

In order to correctly reference this scholarly work, feel free to copy and paste the following:

Tajji Ikawa (2012). AFM Imaging of Biological Supramolecules by a Molecular Imprinting-Based Immobilization Process on a Photopolymer, Atomic Force Microscopy Investigations into Biology - From Cell to Protein, Dr. Christopher Frewin (Ed.), ISBN: 978-953-51-0114-7, InTech, Available from:
<http://www.intechopen.com/books/atomic-force-microscopy-investigations-into-biology-from-cell-to-protein/afm-imaging-of-biological-supramolecules-by-a-molecular-imprinting-based-immobilization-process-on-a>

INTECH
open science | open minds

InTech Europe

University Campus STeP Ri
Slavka Krautzeka 83/A
51000 Rijeka, Croatia
Phone: +385 (51) 770 447
Fax: +385 (51) 686 166
www.intechopen.com

InTech China

Unit 405, Office Block, Hotel Equatorial Shanghai
No.65, Yan An Road (West), Shanghai, 200040, China
中国上海市延安西路65号上海国际贵都大饭店办公楼405单元
Phone: +86-21-62489820
Fax: +86-21-62489821

© 2012 The Author(s). Licensee IntechOpen. This is an open access article distributed under the terms of the [Creative Commons Attribution 3.0 License](#), which permits unrestricted use, distribution, and reproduction in any medium, provided the original work is properly cited.

IntechOpen

IntechOpen